C103-E420

SHIMADZU
Excellence in Science

FTIR
TALK LETTER

Vol. 41

Design of Composites by Grafting Polymer onto Inorganic Particles

School of Materials and Chemical Technology, Tokyo Institute of Technology
Masatoshi Tokita, Professor

1. Introduction

Organic polymers, which are lightweight and easy to mold and process, can be designed with various properties by organic chemistry. However, organic polymers have smaller dielectric constants and thermal conductivities than inorganic substances, and the values can barely be increased. One approach to improving these properties for organic polymer materials is to prepare composite materials comprising organic polymers and inorganic materials. The simple mixing of inorganic particles with organic polymers leads to particle aggregation, which affects the physical properties and moldability of the composite. Homogeneous dispersion of nanosized particles in a polymer matrix by preventing the aggregation yields transparent composite films. Herein, we designed a transparent, high dielectric constant composite film of small barium titanate (BT) particles, an inorganic material with a high dielectric constant $\varepsilon \sim 5000$, dispersed in a matrix of transparent organic polymer, polymethylmethacrylate (PMMA). BT particles were prevented from aggregation by grafting PMMA at high density to the particle surface.[1] We also designed a highly thermally conductive composite comprising a liquid crystal (LC) polymer and magnesium oxide particles, an inorganic material with a high thermal conductivity. In the composite, LC polymer chains grafted onto the particle surface control the LC orientation at the particle surface.[2] These works were conducted utilizing IR spectroscopy.

2. High Permittivity Transparent Films

Touch panels determine the position of the user's finger with a capacitor that forms between the finger and an electrode across a high dielectric constant glass substrate. Replacing this glass substrate with a transparent polymer film will make the touch panels lighter and unbreakable, decreasing the number of persons carrying smartphones with the touch panels broken. High permittivity (dielectric) and transparent polymer composite film can be made of a composite of high dielectric ceramic nanoparticles and a transparent polymer. Ceramic particles have a low affinity for organic polymers due to their high surface energy. Doping surfactants can disperse ceramic particles, but free surfactants can cause leakage current, increasing dielectric losses. We developed a BT-PMMA composite (Fig. 1) by grafting PMMA chains to the particle surface of BT. The PMMA chains grafted on the surface of the BT particles are assumed to prevent the BT particles from aggregating.

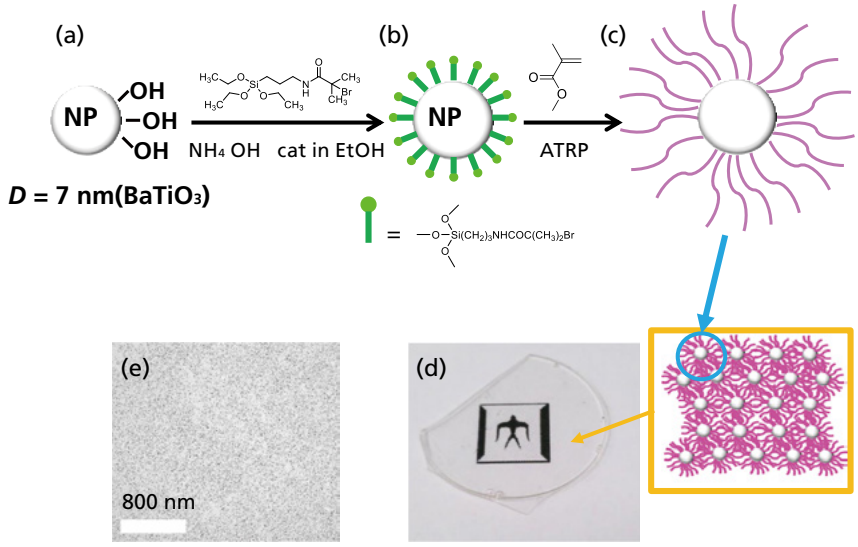

Fig. 1 Preparation of BT-PMMA Composite
(a) BT particle, (b) BT particles coated with surface initiator (BT-Br), (c) PMMA-grafted BT particle (BT/PMMA), (d) photograph of hot-pressed PMMA-grafted BT particles (10% BT by volume), and (e) electron microscopy image of (d). Reproduced with permission from Elsevier.[1]

The BT-PMMA composite was prepared by binding an initiator for atom transfer radical polymerization (ATRP) to the surface of the BT particles (particle diameter D = 7 nm, Fig. 1a and 1b) via a silane coupling reaction then polymerizing methyl methacrylate by the ATRP method (Fig. 1c). BT particles grafting PMMA chains with an average molecular weight of 32,000–40,000 daltons at 0.2–0.7 chains per 1 nm^2 composed a BT-PMMA composite having BT at volume fractions (φ) in the range of 3.2–10 %. All the PMMA chains bonded to the BT particle surface. A hot-pressed composite film had a transparency of 80 % or higher at 550 nm (standardized to 100 µm thickness), allowing a 0.5 mm-thick film transparent (Fig. 1d). The electron microscopy of the film inside disclosed that BT particles were homogeneously distributed in a PMMA matrix (Fig. 1e). Diffuse reflectance (DR) IR spectroscopy allowed us to determine the chemical structures on the surface of the BT particle during composite preparation: the DRIR spectrum measured for BT-Br (BT particles with ATRP initiators grafting onto the surface) included peaks at 1,116 cm^{-1} and 1,020 cm^{-1} that related to Si-O and Si-O-Si, showing the siloxane moiety of the silane coupling agent was bound to the BT particle surface by silane coupling (Fig. 2b). The DRIR spectrum of BT-PMMA (Fig. 2c) included absorption peaks at 2,962 cm^{-1} (C-H stretch), 1,730 cm^{-1} (C=O stretch), and 1,263 cm^{-1} (C-O stretch) related to PMMA chains.

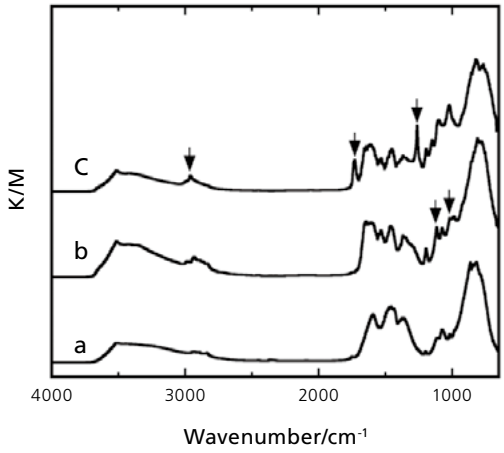

Fig. 2 DRIR Spectra of (a) BT Particles, (b) BT-Br, and (c) BT-PMMA
Arrows in the figure refer to the peaks mentioned in the text. Reproduced with permission from Elsevier.[1]

The BT-PMMA composite film increased ε with φ, reaching ε = 4.1 and tan δ = 0.04 at φ = 10% (25°C, 1 kHz) (Fig. 3a). Interestingly, this suggests that the BT particle has ε = 47, 1/150 the ε value commonly known for BT. This small ε value is attributed to the small size of the BT crystals. Plotting the values of ε against D along with literature data showed that small BT particles have $\varepsilon \propto D^{1.6}$ (Fig. 3b). Adopting larger BT particles will allow us to develop a higher permittivity transparent film by the same procedure; however, BT particles with 20 nm in diameter that we got at that time would have different surface chemical structures, preventing us from grafting PMMA to the particles.

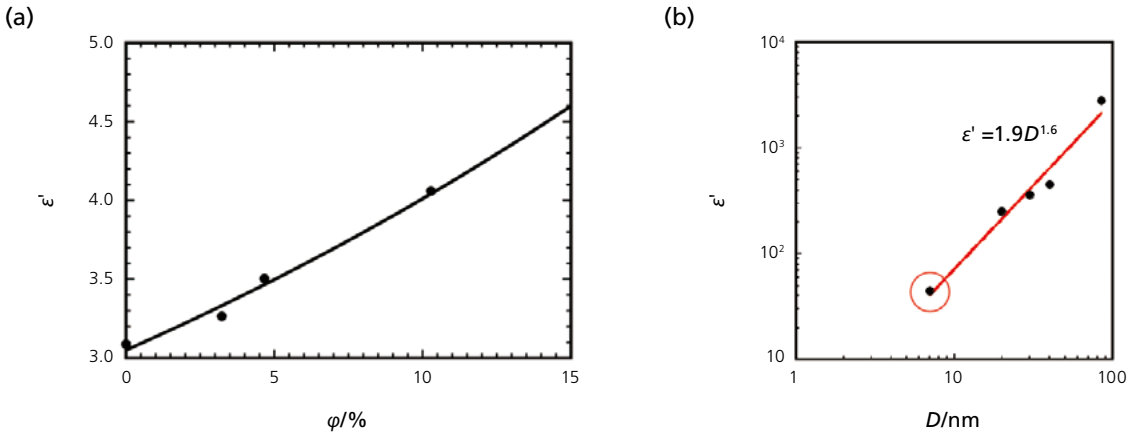

Fig. 3 (a) Dependence of relative permittivity ε of BT-PMMA (1 kHz, 25 °C) on volume fraction φ of BT. The solid line shows ε values calculated using the logarithmic mixing rule and assuming the ε value of BT to be 47. Reproduced with permission from Elsevier.[1]
(b) Dependence of ε on particle diameter (D) for small BT particles. The data in the red circle was collected through this research. All other data points are from the literature.[3, 4]

3. Highly Thermally Conductive Polymer Composites using Liquid Crystal Polymers

Organic polymers typically have much lower thermal conductivities (λ) of ~0.2 W m^{-1} K^{-1}, ~1/1000 than metals. High-λ polymer composites comprise polymer and high-λ inorganic particles (filler). The λ values of these composites (= λ_c) can be estimated from the λ of values of the filler and matrix polymer (λ_f and λ_m) using Equation (1) based on the Bruggeman model.

$$1 - v = \frac{\lambda_c - \lambda_f}{\lambda_m - \lambda_f}\left(\frac{\lambda_m}{\lambda_c}\right)^{1/3} \qquad (1)$$

where v is the volume fraction of filler. The three curves in Fig. 4 show λ_c thus calculated and plotted against v for three composites A–C with different values of λ_f and λ_m. Curve A plots λ_c for composite A with typical values of λ_f and λ_m (λ_f = 30 W m^{-1} K^{-1}, λ_m = 0.2 W m^{-1} K^{-1}). Curves B and C show λ_c for composites B and C with λ_f and λ_m, respectively, five times the value for composite A. These curves demonstrate that improving the thermal conductivity of the polymer is effective in improving λ_c. For example, to achieve λ_c = 2 W m^{-1} K^{-1}, composites A and B must have the filler at v = 55 %, which is more than twice v for composite C (v = 25 %).

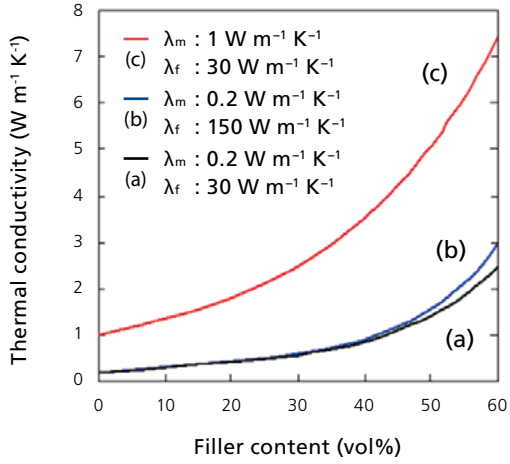

Fig. 4 Thermal conductivity of polymer composite (λ_c) calculated based on Bruggeman model (eq. (1)) and plotted against the volume fraction of filler particles (v) for the composite comprising a polymer and filler particles with thermal conductivities λ_m and λ_f, respectively. (a) λ_m = 0.2 W m^{-1} K^{-1} and λ_f = 30 W m^{-1} K^{-1}; (b) λ_m = 0.2 W m^{-1} K^{-1} and λ_f = 150 W m^{-1} K^{-1}; (c) λ_m = 1 W m^{-1} K^{-1} and λ_f = 30 W m^{-1} K^{-1}. Reproduced with permission from the American Chemical Society.[2]

Although organic polymers typically have a very low λ, they often have high λ in the polymer chain direction when the chains are stretched. For example, high λ values have been reported for polyethylene in the form of highly stretched films (62 W m^{-1} K^{-1}) [5] and nanofibers (104 W m^{-1} K^{-1}).[6] Extended polymer chains are thought to conduct heat well along their covalent bonds. In this context, liquid crystal polymers (LCPs) also have a high λ in the director orientation because LCPs extend the polymer chains along the director orientation. Higher thermal conductivities in the director orientation have been reported even for low-molecular-weight liquid crystals and side-chain polymer liquid crystals; however, these have no covalent bond lying along the director orientation.[7–9] We designed an LCP composite having λ_m comparable to λ measured in the direction of LCP orientation ($\lambda_{//}$). The LCP chains grafting on the filler surface extending from the surface (Fig. 5a) orient the director orientation of the LC matrix perpendicular to the filler surface. The LC between the filler surfaces smoothly varies the director orientation, forming heat paths with a thermal conductivity of $\lambda_{//}$ between the fillers (Fig. 5b).

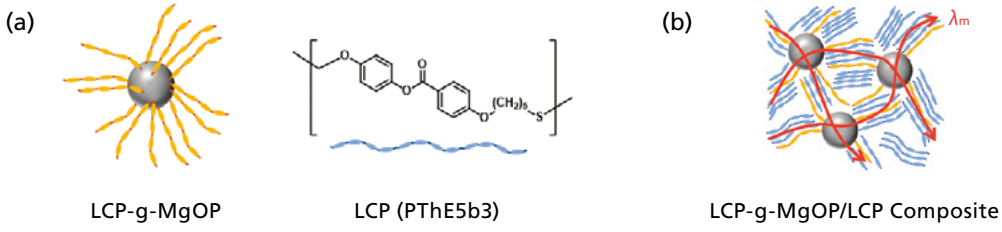

Fig. 5 (a) Magnesium oxide particle with liquid crystal PThE5b3 polymer grafting onto the surface (LCP-g-MgOP) and the chemical structure of PThE5b3. (b) Schematic of liquid crystal director orientation arrangement and heat transfer paths in the LCP-g-MgOP/LCP composite. Reproduced with permission from the American Chemical Society.[2]

LCP-g-MgOP were prepared by grafting a liquid crystal PThE5b3 polymer onto the surface of magnesium oxide particles modified with allyl groups (MgOP, particle diameter 10 μm) (Fig. 5a). PThE5b3 forms a smectic liquid crystal with $\lambda_{//}$ = 0.64 W m^{-1} K^{-1} at 25 °C. The monomer of PThE5b3 has a thiol group and an allyl group at each end, which react with each other to form the polymer. Polymerizing the monomer in the presence of allyl-functionalized MgOP allowed PThE5b3 to graft onto the surface, yielding LCP-g-MgOP (MgOP with PThE5b3 grafted to the surface) as well as the free PThE5b3 polymer. The allyl groups on MgOP react with the thiol group, bonding the monomers to MgOP. The monomers bind to those on the surface or each other to form polymer chains that graft from the particle surface and free polymer chains. LCP-g-MgOP was recovered from the mixture with the free polymer by repeated dispersion, washing, and centrifugation in a good solvent for the polymer and analyzed by FTIR spectroscopy. The FTIR spectrum showed peaks attributed to PThE5b3 and MgOP (Fig. 6a). For example, peaks at 3,700 (O-H stretch), ~1500, ~850, and ~500 cm^{-1} (Mg-O stretch) (Fig. 6b) have been observed for MgOP and peaks at 3,055 cm^{-1} (Ar-H stretch), 2,930 and 2,850 cm^{-1} (CH_2 stretch), 1,730 cm^{-1} (C=O stretch), and 1,600 and 1,500 cm^{-1} (aromatic C=C stretch) for PThE5b3 (Fig. 6c). Comparing these IR spectra allowed us to confirm the chemical composition of LCP-g-MgOP. The weight fraction of PThE5b3 in LCP-g-MgOP was determined to be 15 wt% by thermal gravimetry (TG).

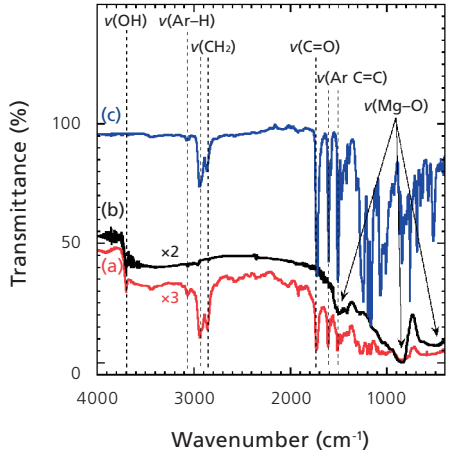

Fig. 6 DRIR Spectra of (a) LCP-g-MgOP and (b) MgOP and ATR-IR Spectrum of (c) PThE5b3
Reproduced with permission from the American Chemical Society.[2]

The $\lambda_{//}$ value of PThE5b5 was determined to be 0.635 W m^{-1} K^{-1} using the thermal diffusivity α measured for a magnetically oriented sample along the director orientation by temperature wave analysis and the relationship between λ and α ($\lambda = \alpha\rho C_P$, where ρ is density and C_P is heat capacity at constant pressure). The LCP-g-MgOP/LCP composite at a MgOP volume fraction (v) of 34 % had λ_c = 2.1 W m^{-1} K^{-1}, allowing us to estimate the λ_m value to be 0.66 W m^{-1} K^{-1} using Eq. (1) and the λ value of MgO (42 W m^{-1} K^{-1}). This λ_m value is comparable to the $\lambda_{//}$ value determined for the oriented LCP sample along the director orientation. It indicates that the λ of LCP composites can be efficiently enhanced by controlling the liquid crystal orientation on the filler surface. The λ_m can be increased to be as high as $\lambda_{//}$, the highest λ of the LCP measured in the director orientation. This finding allows us to increase the λ_c of the LCP composites efficiently, providing a design for a high thermal conductivity polymer composite using LCPs.

4. Conclusion

We used polymer-grafted inorganic particles to design high-performance functional polymer composites. FTIR spectroscopy allowed us to conduct experiments efficiently by rapidly analyzing the chemical structure on the particle surfaces in the laboratory.

Acknowledgments

This research was supported by JST S-INNOVATION "Development of new device technology through controlling polymer nano-orientation" (2009–2018) and JST-CREST "Materials informatics of thermophysical properties of polymers" (JPMJCR19I3).

References

[1] N. Iwata, O. Sato, K. Ohno, K. Sakajiri, S. Kang, and M. Tokita, *Polymer*, **81**, 23–28 (2015).

[2] S. Ishikawa, K. Kawahara, S. Tomizawa, Y. Watanabe, and M. Tokita, *ACS Appl. Polym. Mater.*, **4**, 6908–6915 (2022).

[3] T. Hoshina, H. Kakemoto, T. Tsurumi, S. Wada, and M. Yashima, *J. Appl. Phys.*, **99**, 1–9 (2006).

[4] P. Kim, N.M. Doss, J.P. Tillotson, P.J. Hotchkiss, M. Pan, S.R. Marder, J. Li, J.P. Calame, and J.W. Perry, *ACS Nano*, **3**, 2581–2592 (2009).

[5] Y. Xu, D. Kraemer, B. Song, Z. Jiang, J. Zhou, J. Loomis, J. Wang, M. Li, H. Ghasemi, X. Huang, X. Li, and G. Chen, *Nat. Commun.*, **10**, 1771 (2019).

[6] S. Shen, A. Henry, J. Tong, R. Zheng, and G. Chen, *Nat. Nanotechnol.*, **5**, 251–255 (2010).

[7] M. Uehara, H. Takezoe, N. Vaupotič, D. Pociecha, E. Gorecka, Y. Aoki, and J. Morikawa, *J. Chem. Phys.*, **143**, 074903 (2015).

[8] A. Sugimoto, Y. Yoshioka, S. Kang, and M. Tokita, *Polymer*, **106**, 35–42 (2016).

[9] H. Harada, T. Saito, and M. Tokita, *Macromolecules*, **55**, 1178–1184 (2022).

Laser Light Sources Used in Raman Spectroscopy

Spectroscopy Business Unit, Analytical & Measuring Instruments Division
Tomoyo Tao

The AIRsight Infrared/Raman Microscope, launched in November 2022, uses two lasers of different oscillation wavelengths as light sources for Raman analysis. Lasers are also used in Fourier transform infrared (FTIR) spectrophotometers, but while Raman spectroscopy uses lasers as a light source, FTIR systems use lasers for data sampling of IR spectra. So why does Raman analysis use lasers and why is the AIRsight equipped with two lasers? This article focuses on the lasers used as light sources in Raman spectroscopy, and introduces the two lasers equipped in AIRsight along with examples of Raman measurement.

1. Light Sources in Raman Spectroscopy

Why are lasers used as a light source in Raman spectroscopy? Because the monochromaticity and high-power output of lasers are extremely useful for Raman analysis. This section explains why lasers are an excellent light source for Raman analysis.

IR spectroscopy irradiates a sample with an IR light source and observes absorption of incident light by the functional groups in the sample. Because the wavelength (wavenumber) of the absorbed light differs depending on the type of functional groups, IR spectroscopic analysis requires a light source with a broad wavelength range. Meanwhile, Raman spectroscopy irradiates a sample with a laser and observes the Raman scattered light generated from the sample by the incident light. More specifically (Fig. 1), Raman spectroscopy gets information on the fundamental vibrations of a molecule (ν_1) using the wavenumber difference (Raman shift) between Rayleigh scattered light, which has the same wavelength as the excitation light (wavenumber: ν), and Raman scattered light from the sample (frequency: $\nu - \nu_1$ or $\nu + \nu_1$).

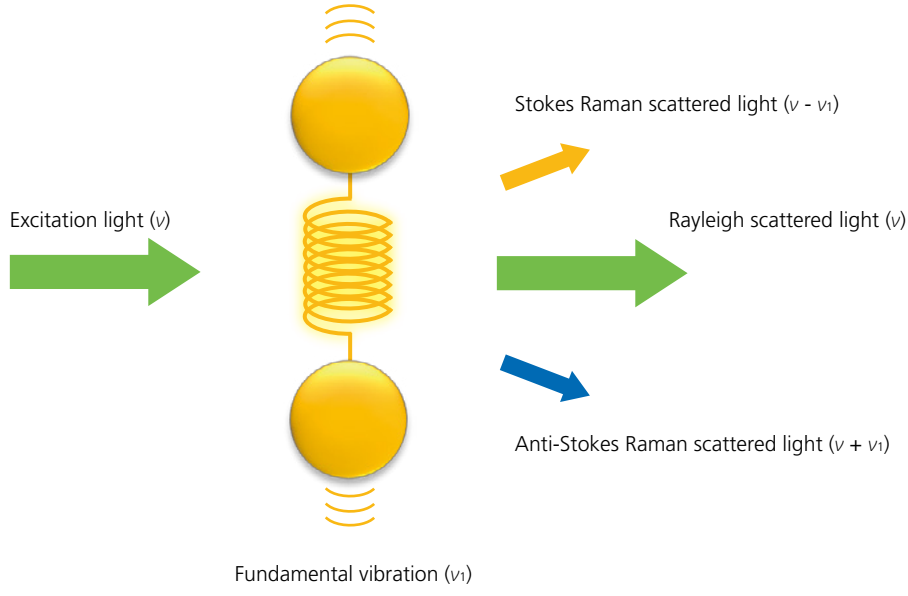

Fig. 1 Basic Principle of Raman Spectroscopy

To acquire high-resolution Raman spectra, the Raman scattered light and incident light must have a narrow linewidth (wavelength spread). As shown in Fig. 2, when incident light with a broad linewidth is used, Raman scattered light with a broad linewidth is generated and the spectrum resolution decreases. To avoid this, rather than the natural light or IR light source with a wide wavelength range, Raman spectroscopy needs a narrow-band light source that emits a single wavelength. This is why the lasers with monochromaticity are excellent light sources for Raman spectroscopy.

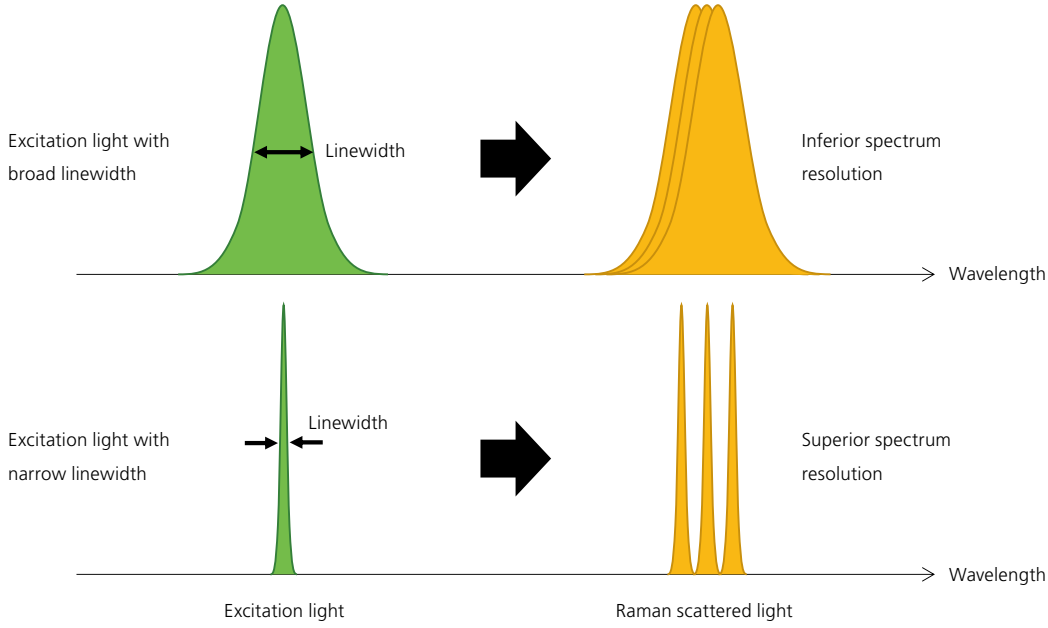

Fig. 2 Relationship between Excitation Light Linewidth and Raman Spectrum Resolution

Raman scattered light is very weak, with an intensity of around 10^{-6}, the power of the incident light. Because Raman scattered light intensity is proportional to the intensity of the light source, the greater the light source intensity the easier it is to detect Raman scattered light. Therefore, in addition to requiring a highly sensitive detector, Raman spectroscopy also requires a high-power light source. Being high-power light sources, lasers are also excellent light sources for Raman spectroscopy from this perspective (though power outputs must be chosen with care as some samples are damaged and burned by high-power lasers).

Due to the need for a high-power light source with a narrow linewidth as outlined above, lasers are widely used in Raman spectroscopy. In addition to their monochromaticity and power, the directionality and polarization properties of lasers also make them excellent light sources for Raman spectroscopy. Please see the textbooks referenced at the end of this article for more information on this topic[1)–3)].

2. Lasers Used by AIRsight

This section covers the lasers installed in AIRsight (Fig. 3) and correction functions related to these lasers.

Raman spectrometers and Raman microscopes typically use gas lasers and solid-state lasers as light sources. AIRsight uses diode pumped solid-state lasers that save space. These laser modules were designed by the Device Department at Shimadzu.

Because the slightest fluctuation in the oscillation wavelength of incident light causes a shift in the wavenumbers of the resulting Raman spectra, the lasers used in Raman analysis must have high wavelength stability. The lasers used by AIRsight are equipped with a temperature control function that ensures high wavelength stability by adjusting for slight wavelength shifts derived from environmental temperature variations. AMsolution, the control software for AIRsight, is also equipped with a correction function that uses known peak positions and the peak positions in a Raman spectrum acquired from a polystyrene sample to identify shifts in wavenumber and correct the horizontal wavenumber axis. This correction is undertaken by Shimadzu field engineers at system installation but can also be performed by the user as a part of routine system inspection.

The quality of Raman spectra is also affected by optical axis stability. Because AIRsight is a confocal optical microscope, even the slightest shift of the laser's optical axis has a major effect on Raman spectrum intensity. For this reason, the lasers used by AIRsight feature excellent emission angle stability. Any misalignment of the optical axis due to external factors such as optical elements or holders unrelated to the lasers is corrected by the automatic Raman adjustment function in AIRsight. This function optimizes the optical axis of the laser and Raman scattered light by automatically adjusting the angle of mirrors on the optical axis of each to correct very slight misalignments in the optical axis of the laser.

Fig. 3 FTIR System (IRXross) and AIRsight

3. Laser Safety

Lasers are classified based on power output and wavelength range. The lasers used by AIRsight are classified as Class 3B laser products by the International Electrotechnical Commission (IEC 60825-1:2014) and Japanese Industrial Standards (JIS C6802:2014). Class 3B lasers have a high-power output (not more than 0.5 W) that makes direct eye exposure dangerous and irradiation of the skin to be avoided. The lasers in AIRsight come with an interlock function that prevents irradiation to samples while the light-shielding cover for the AIRsight sample stage is open. Because of this function, even though AIRsight uses Class 3B lasers, the AIRsight system itself is classified as a Class 1 laser product. Class 1 laser products are intrinsically safe, require no special safety measures, and can be used without concern for laser exposure.

4. Lasers of Different Wavelengths

As mentioned above, AIRsight is equipped with two lasers of different oscillation wavelengths (center wavelengths of 532 nm and 785 nm). But why is AIRsight equipped with two lasers? And how does irradiating a sample with lasers of different oscillation wavelengths affect the resulting Raman spectrum? This section looks at the effect of different laser oscillation wavelengths on the Raman spectrum.

(1) Raman Signal Intensity

The intensity of Raman scattered light is proportional to the fourth power of the excitation light frequency. Even if two lasers have the same power output, the laser with the shorter wavelength will produce scattered light with higher intensity. Accordingly, Raman spectrum signals can be generated more effectively with shorter wavelength lasers.

(2) Impact of Fluorescence

Some samples fluoresce in response to laser irradiation. The fluorescence emissions from these samples often create a broad signal that overlaps the entire spectrum and weak Raman signals may be buried in this fluorescence signal, resulting in no meaningful Raman spectra. For this reason, fluorescence is a significant issue in Raman spectroscopy. Since shorter wavelength lasers such as 532 nm lasers are more likely to produce fluorescence, if irradiation with a shorter wavelength laser causes fluorescence, the effects can be mitigated by switching to a longer wavelength laser such as a 785 nm laser.

Also, because fluorescence tends to fade with prolonged laser irradiation, a "photo-bleaching" function is included in AIRsight that commences measurements after the sample is irradiated for a set duration. This function also offers an effective means of reducing the impact of fluorescence.

(3) Measurable Wavenumber Range (Detection Sensitivity of CCD Detector)

Since Raman shift is the difference in wavenumber between incident light and Raman scattered light, when a different excitation light wavelength is used to observe the same Raman shift, the resulting Raman scattered light will be of a different wavelength. In the example shown in Fig. 4, when observing in the wavenumber region of 3,000 cm^{-1} where C-H stretching vibrations are detected, an excitation wavelength of 532 nm results in a Raman scattered light wavelength of 633 nm and an excitation wavelength of 785 nm results in a Raman scattered light wavelength of 1,026 nm. Note how the shift in wavenumber between excitation light and Raman scattered light is 101 nm in the former case and 241 nm in the latter case. The shorter the laser wavelength, the narrower the wavelength range of Raman scattered light and the longer the laser wavelength, the wider the wavelength range of Raman scattered light. In AIRsight, though the same detector is used to detect Raman scattered light from 532 nm and 785 nm laser excitation, the sensitivity of the detector is wavelength-dependent and decreases at longer wavelengths. Specifically, for a peak at around 3,000 cm^{-1}, the detector sensitivity for Raman scattered light using 785 nm excitation is 1/5 that for Raman scattered light using 532 nm excitation. This is why 532 nm excitation is recommended over 785 nm excitation when looking to detect high wavenumber peaks with good sensitivity.

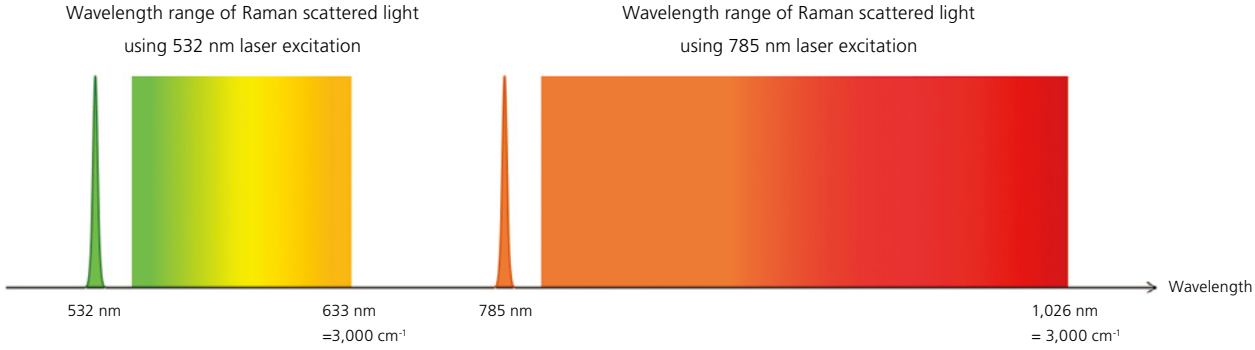

Fig. 4 Measurable Wavenumber Range by Laser

(4) Sample Damage Threshold

The threshold laser intensity at which a given sample is damaged by laser irradiation depends on the laser's wavelength. The threshold is higher for longer wavelength lasers compared to shorter wavelength lasers, hence 785 nm laser excitation can be used to reduce the likelihood of burning samples that are vulnerable to damage.

So far, this article has described the relationship between the laser oscillation wavelength and Raman spectra from four points of view. When we compare the characteristics of a 532 nm laser and a 785 nm laser, they point to 532 nm laser excitation being more effective overall due to the higher intensity of Raman scattered light and better detection sensitivity at higher wavenumbers, while 785 nm laser excitation would be suited to samples that emit fluorescence and are susceptible to burning. Since each laser wavelength has its advantages and disadvantages, AIRsight is equipped with both lasers to ensure optimum performance in all situations. Simply select the laser wavelength that best suits your sample and analysis objectives.

5. Raman Spectra Obtained by 532 nm and 785 nm Laser Excitation

While the previous section described the effects of different laser wavelengths in theory, this section presents Raman spectra obtained using 532 nm and 785 nm laser excitation and actual samples.

(1) Effect of CCD Detector Sensitivity on Raman Peak Intensity

As touched on in the previous section, in the case of 785 nm excitation, the detector sensitivity in the high wavenumber range is markedly lower compared with that of 532 nm excitation. We attempted to ascertain this difference in sensitivity by measuring the Raman spectra of polystyrene (PS), a material used as a reference sample in Raman analysis. Fig. 5 shows Raman spectra of PS measured using both a 532 nm laser and a 785 nm laser. Note that the spectra have been normalized to the peak intensity at 1,001.4 cm^{-1}.

The spectra show that high peak intensity originating from C=C-H stretching vibrations in PS is detected at 3054.3 cm^{-1} when using the 532 nm laser, but the same stretching vibrations are barely detected using the 785 nm laser.

(2) Mitigating the Impact of Sample Fluorescence

This section uses measurement data obtained from acrylonitrile butadiene styrene (ABS). Fig. 6 shows Raman spectra of ABS obtained using both a 532 nm laser and a 785 nm laser.

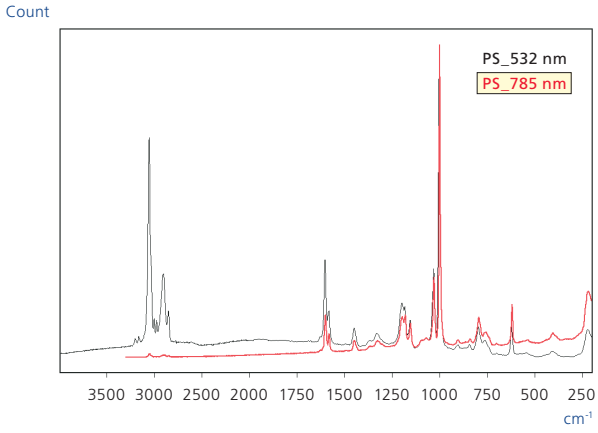

Fig. 5 Raman Spectra of PS
(Black line: 532 nm excitation, red line: 785 nm excitation)

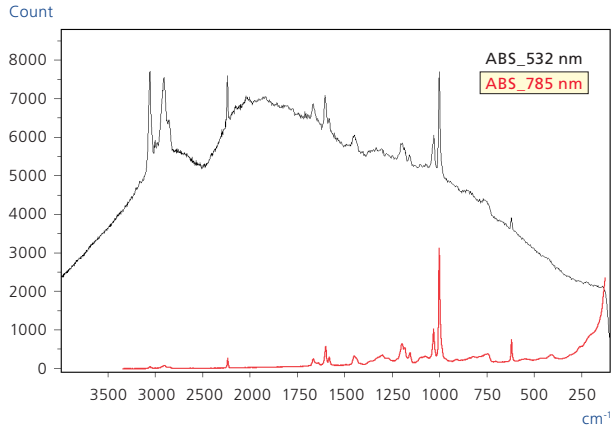

Fig. 6 Raman Spectra of ABS
(Black line: 532 nm excitation, red line: 785 nm excitation)

In the case of 532 nm excitation, we can see that the baseline of the spectrum is markedly raised over the whole wavenumber range due to the impact of fluorescence. By contrast, 785 nm excitation gives a good Raman spectrum with a flat baseline and no impact from fluorescence. Although the impacts of fluorescence were avoided in this example by switching the excitation wavelength from 532 nm to 785 nm, switching to 785 nm may not fully eliminate the impact of fluorescence in every case. In these instances, the impact of fluorescence can be minimized by irradiating the laser to the sample for a set duration before commencing spectral measurements, as was touched on earlier in this article.

Application News No. 01-00586 presents an example analysis of UV-degraded ABS using 532 nm excitation and 785 nm excitation and can be referred to for further insights into this topic.

6. Conclusion

This article touches on lasers used as light sources in Raman spectroscopy, describes the correction functions of laser oscillation wavelength equipped in the AIRsight IR/Raman microscope, and presents measurement data of Raman spectra with different laser oscillation wavelengths.

We hope this article will help you select the best laser wavelength for Raman analysis and provide some insight into the exceptional features of AIRsight.

References

[1] Hiroo Hamaguchi and Akiko Hirakawa, The Spectroscopical Society of Japan Measurement Methods Series 17: Raman Spectroscopy, Gakkai Shuppan Center (1994)

[2] Hiroo Hamaguchi and Koichi Iwata, Spectroscopy Series 1: Raman Spectroscopy, Kodansha (2015)

[3] Toshikatsu Nishioka, Infrared and Raman Spectroscopy of Polymers, Kodansha (2016)

Notes on Infrared Spectral Analysis – The Fundamentals –

Solutions COE, Analytical & Measuring Instruments Division
Shoko Iwasaki, Yasushi Suzuki

When it comes to analyzing data acquired by Fourier transform infrared (FTIR) spectrophotometer, an increasing number of databases and software search tools, which offer increasingly refined algorithms and improved ease-of-use, have simplified spectral searches and trivialized the work required to display those results on a PC screen. But deciding whether the results given by such software are correct remains work for analysts, and substantial knowledge is required to properly execute that work.

Focusing on fundamental aspects of FTIR, this article explores the vertical axis of the IR spectrum, varieties and characteristics of molecular vibration, and absorption bands characteristic to common functional groups. Further articles in this series also plan to cover individual functional groups in more detail.

1. Ordinate of the Infrared Spectrum

While FTIR data can be presented as a transmittance spectrum or an absorption spectrum, which of these presentations should be used for analysis? This section explores these two methods of presenting FTIR data.

Fig 1 shows multiple IR spectra of ethanol in which one spectral profile is a good spectrum and the other profile shows peak saturation. The top figure shows data presented as transmittance spectra and the bottom figure as absorption spectra.

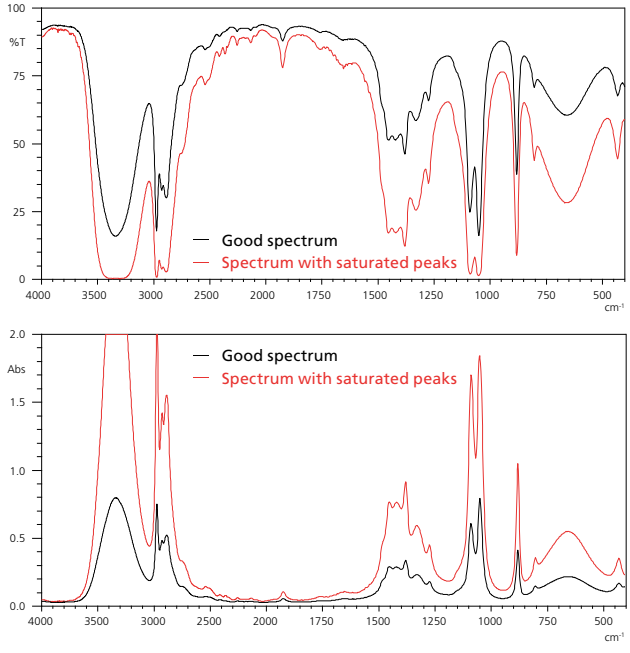

Fig. 1 Infrared Spectra of Ethanol
(Top: Transmittance Spectra, Bottom: Absorption Spectra)

The good spectrum profile (black line) of both the transmittance (top) and absorption (bottom) spectra has clearly identifiable peaks in the same positions. This demonstrates that when the spectrum is good, FTIR data can be analyzed as either a transmittance or absorption spectrum without affecting the results.

Looking at the transmittance and absorption spectra with saturated peaks (red lines), the transmittance spectrum shows almost total peak saturation at around 3,000 cm^{-1} and 1,050 cm^{-1}, making the positions of these peaks difficult to determine. Also, compared to the transmittance spectrum, the spectral features of the absorption spectrum with saturated peaks are more identifiable across the entire spectral range. This difference is explained by the Lambert-Beer law shown below.

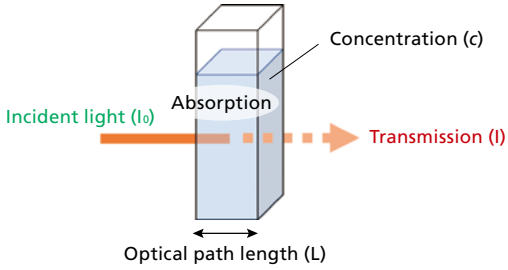

Fig. 2 Schematic Image of Transmission

As shown in Fig. 2, IR light incidents at intensity I_0 and is transmitted by the sample at intensity I. In this case, sample transmittance and absorbance can be represented by the following equations.

Transmittance $T(\%)\equiv(I/I_0)=10^{-\varepsilon cL}$ ⋯ Equation (1)

Absorbance $A\equiv\log_{10}(I_0/I)=\log_{10}10^{\varepsilon cL}=\varepsilon cL$ ⋯ Equation (2)

ε: molar absorption coefficient, c: concentration (mol/L), L: optical path length (cm), λ: wavelength

Based on equations (1) and (2), the relationship between transmittance and absorbance can be represented by Equation (3) below.

$A\equiv\log_{10}(1/T)$ ⋯ Equation (3)

This shows a logarithmic relationship between the absorbance spectrum and transmittance spectrum; hence, when data is presented in a transmittance spectrum the effects of saturation tend to collapse stronger peaks. Conversely, very weak peaks that are difficult to identify in an absorbance spectrum are more identifiable when presented in a transmittance spectrum. To summarize,

1. Either the transmittance spectrum or absorbance spectrum can be analyzed without issue if the acquired spectrum is good and has no peak saturation
2. If the spectrum is saturated, the absorbance spectrum is superior for interpreting the overall spectral profile
3. Very weak peaks in the transmittance spectrum can be made larger by saturating the spectrum.

It is best practice to use the spectrum that best suits the intended analysis.

In a related but separate point, since Equation (1) shows transmittance is not proportional to concentration, the transmittance spectrum is not suitable for quantitative analysis by FTIR.

2. Fundamental Molecular Vibrations

When organic compounds and some inorganic compounds are irradiated with IR light, the interaction between the IR light, and molecules of the substance creates vibrations in the molecules. These vibrations are caused by movement by the atoms that make up the molecule. While molecules with few atoms exhibit only a small variety of vibrations, polyatomic molecules with many atoms exhibit a large variety of complex vibrations. This article introduces the normal modes of these molecular vibrations.

The normal modes of vibration are illustrated in Fig. 3. Fundamental vibrations (normal modes) are broadly separated into stretching vibrations that lengthen and shorten the distance between atoms and deformation vibrations that change the angle between atoms. Stretching vibrations are further separated into symmetric and asymmetric stretching, and deformation vibrations are separated into scissoring (in-plane), rocking (in-plane), twisting (out-of-plane), and wagging (out-of-plane) vibrations.

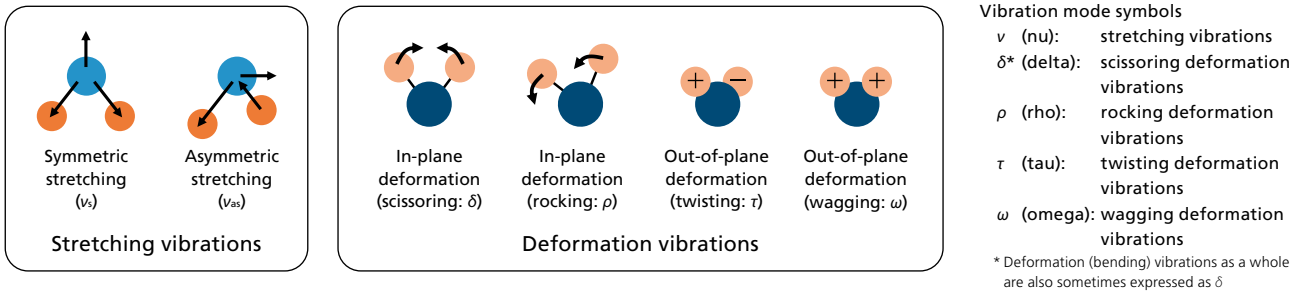

Fig. 3 Fundamental Molecular Vibrations (Normal Vibration Modes)

However, not all these fundamental vibrations can be detected by light absorption. Three reasons why peaks are not detected by IR spectroscopy are outlined as follows. First, the vibrations produce absorption peaks outside the measured wavenumber range. This applies to vibrations that absorb light outside the mid-IR range between 4,000 cm^{-1} and 400 cm^{-1}. For example, many inorganic compounds cannot be detected by FTIR because they absorb light in the far IR region below 400 cm^{-1}, though these compounds can be detected by far-IR FTIR. Second, the vibrations have a small coefficient of molar absorption. This occurs when analyzing low-concentration samples. In such cases, concentrating the sample before analysis or applying other sample processing can allow detection. Third is what is termed the IR selection rule. The degree of charge polarity in a molecule is expressed by a physical quantity called a dipole moment, and IR absorption cannot occur if the dipole moment of a molecule does not change during a vibration. As shown in Fig. 4, diatomic molecules containing one type of atom such as nitrogen (N_2) and oxygen (O_2) do not absorb IR because their dipole moment is not changed by vibration. Even molecules with more than one type of atom may not absorb IR, as is the case with carbon dioxide, which experiences symmetric stretching vibrations that do not change its dipole moment. In fact, the reason why IR spectral measurements can be performed in air at all is because nitrogen and oxygen do not absorb IR light.

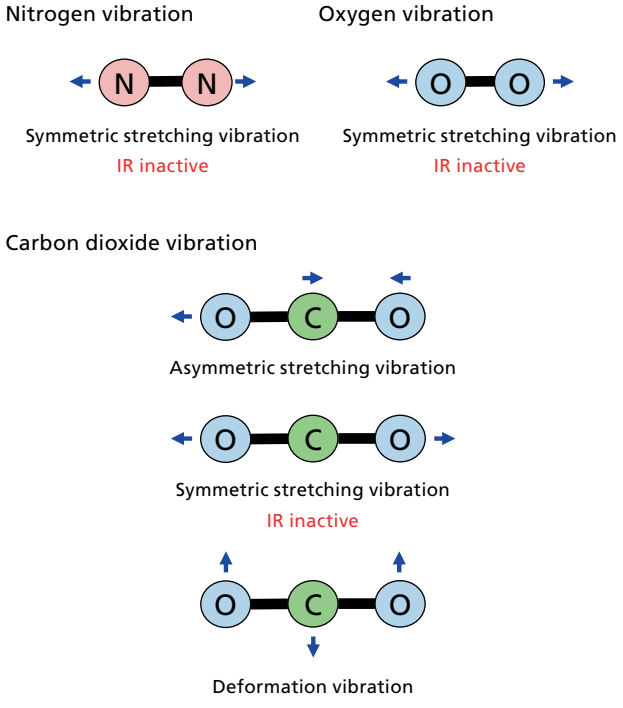

Fig. 4 Vibrations Not Detected Due to IR Selection Rule

We shall now examine the fundamental vibrations of carbon dioxide (CO_2), a linear molecule, and water (H_2O), a nonlinear molecule, as specific examples.

(1) Fundamental Vibrations of Carbon Dioxide (CO_2)

Fig. 5 shows the absorption spectrum and fundamental vibrations of CO_2.

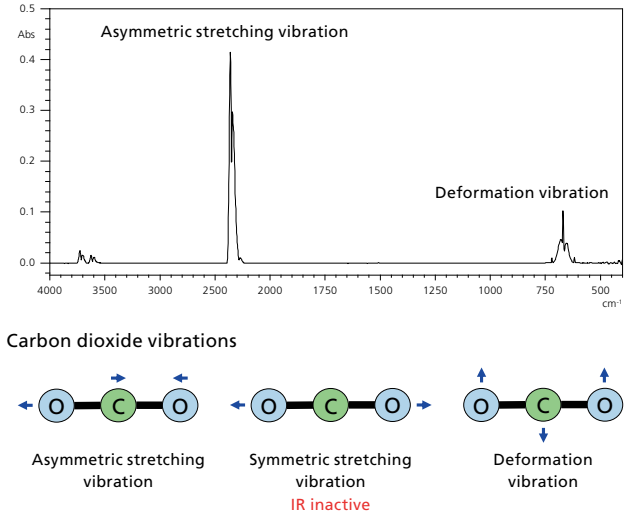

Fig. 5 Absorption Spectrum and Fundamental Vibrations of Carbon Dioxide (CO_2)

Asymmetric stretching vibrations appear at around 2,350 cm^{-1} and deformation vibrations at around 667 cm^{-1}. Theoretical calculations place the peak position of symmetric stretching vibrations at around 1,340 cm^{-1}, but the peak does not appear on the IR spectrum due to the vibrations being IR inactive. These symmetric stretching vibrations of CO_2 are Raman active, but Raman analysis detects them as a peak split into two components at around 1,388 cm^{-1} and 1,286 cm^{-1} due to a phenomenon called Fermi resonance.[1] Two small peaks also appear on the IR spectrum at around 3,700 cm^{-1} and 3,600 cm^{-1}, but these are explained combination tones of the IR active peak at around 2,350 cm^{-1} and the Raman active peaks at around 1,388 cm^{-1} and 1,286 cm^{-1}.[2]

(2) Fundamental Vibrations of Water (H_2O)

Fig. 6 shows the absorption spectrum and fundamental vibrations of water (H_2O).

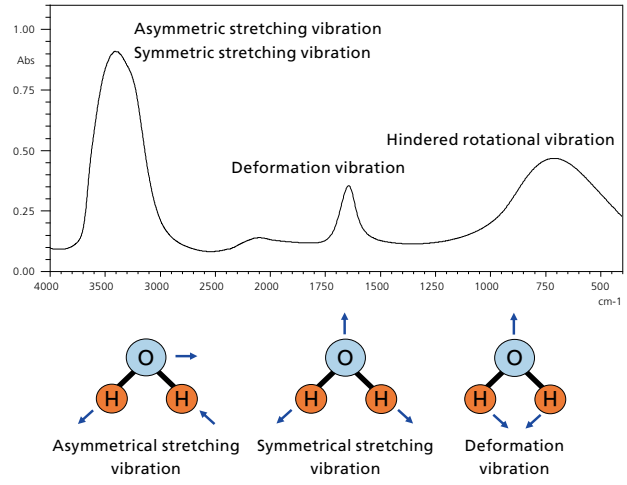

Fig. 6 Absorption Spectrum of Water (H_2O)

Asymmetrical stretching vibrations and symmetric stretching vibrations appear at around 3,400 cm^{-1} and overlap one another. Deformation vibrations also appear at around 1,640 cm^{-1}. When analyzed as a liquid, the rotational spectrum does not appear as the water molecules are in close proximity and unable to rotate freely (the rotational spectrum will be discussed later). Peak intensities, positions, and shapes are also altered by the effects of water molecule condensation, hydrogen bonding between adjacent hydrogen and oxygen atoms, and other phenomena. Note that the peak at the low wavenumber end of the spectrum has been identified as a hindered rotational vibration (libration) and not a fundamental vibration.

Fig. 7 shows the absorption spectrum of water vapor.

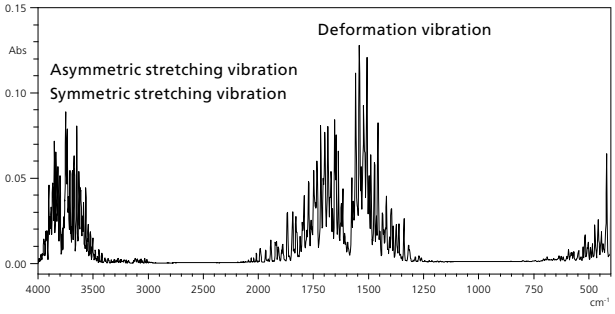

Fig. 7 Absorption Spectrum of Water Vapor

Asymmetric stretching vibrations and symmetric stretching vibrations in water vapor appear at 3,756 cm^{-1} and 3,652 cm^{-1} and deformation vibrations appear at around 1,595 cm^{-1}.[1] Since water vapor is a gas and can rotate freely, the rotational spectrum also appears. The many narrow peaks in the spectrum are caused by the rotational spectrum overlapping the vibrational spectrum. The wavenumbers of fundamental vibrations noted above are obtained from actual measurements and calculations arrived at after a range of experimental efforts. For reference, the peak appearing at the low wavenumber side of the spectrum from around 600 cm^{-1} is not caused by fundamental vibrations but is part of the pure rotational spectrum of water vapor and continues into the far IR region.

Considering the complex fundamental vibrations of molecules with only three atoms such as CO_2 and H_2O, compounds with truly complex structures will produce even more absorption features.

3. Characteristic Absorption Bands of Common Functional Groups

Reference charts such as Colthup charts[3] that show functional groups on the vertical axis and absorption wavenumber bands on the horizontal axis are extremely helpful in IR spectral analysis. However, applying such reference charts to the interpretation of IR spectrum peaks still requires a certain level of experience and knowledge. This section offers some insights and tips that can be applied immediately in your work.

First, reading IR spectra is relatively easy once you remember a few basic rules. Fig. 8 shows the characteristic absorption bands of some of the main functional groups. Since absorption wavenumbers can shift depending on environmental effects around the functional group, the absorption bands are shown as a range.

So which region should we use to interpret absorption spectra? When attempting to identify principle components in a real-world analysis, initially focusing on peaks in the high wavenumber region of the spectrum reduces the number of potential cases and can speed up identification. By contrast, the region below 1,500 cm^{-1}, referred to as the fingerprint region, contains large numbers of absorption features that are unique to compounds but also overlap with each other, making identification more difficult.

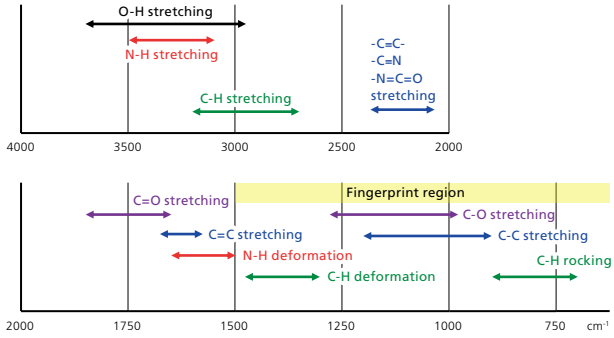

Fig. 8 Characteristic Absorption Bands of Common Functional Groups

4. Conclusion

This article provides an introduction to the basics of IR spectral analysis. The next article in this series will cover the characteristic absorption bands of the major functional groups shown in Fig. 8, including peak position, intensity, width, and other peak characteristics, as well as provide some useful approaches and techniques for analysis.

We hope those thinking of venturing into IR spectroscopy will find this article useful.

References

[1] Shigeyuki Tanaka and Norio Teramae, Infrared spectroscopy, Kyoritsu Shuppan (1993)

[2] Ichiro Nakagawa, Vibrational Spectroscopy, Gakkai Shuppan Center (1987).

[3] N. B. Colthup : J. Opt. Soc. Am. 40, 397 (1950)

The Questions and Answers section has been omitted from this issue due to the circumstances of the publication.

Efficient Thermal Stability Analysis of Nucleic Acid Drugs

Tm Analysis System

Tm analysis serves an important role in checking the thermal stability and sequence of nucleic acids. In Tm analysis, heat is applied to the nucleic acids in double strands. Then, the change in absorbance (melting curve) that occurs as the temperature increases and the strands dissociate into single strands is measured. The melting temperature (Tm value) is determined as the temperature where the mole fractions of single and double strands are equal.

- Automatically determines the melting temperature (Tm) at which 50 % of double-stranded nucleic acids separate into single-stranded nucleic acids
- Minimum sample volume of just 10 µL
- Supports highly robust data integrity
- One-step analysis from spectrum acquisition to Tm determination

Measure spectrum → Anneal → Measure Tm values and analyze data → Calculate Tm values

TMSPC™-8i
8-cell thermoelectrically temperature controlled cell holder

UV-2600i
UV-VIS Spectrophotometer

Product: Tm Analysis System — Application

Oligonucleotide Therapeutics Solution — Application

SHIMADZU

Shimadzu Corporation
www.shimadzu.com/an/